



## Seismic evidence for dilatational source deformations accompanying the 2004–2008 Yellowstone accelerated uplift episode

T. Taira,<sup>1,2</sup> R. B. Smith,<sup>1</sup> and W.-L. Chang<sup>1,3</sup>

Received 31 December 2008; revised 26 June 2009; accepted 14 August 2009; published 2 February 2010.

[1] Dilatational source deformations associated with two unusual  $M$  3+ earthquakes in the area of the 2004–2008 Yellowstone, WY, accelerated uplift episode were identified through detailed analysis of moment tensor inversions. Pressurized hydrothermal fluids are suggested to be associated with the dilatational source processes of these unusual earthquakes, which is consistent with the mechanism of the GPS-InSAR derived deformation signal of the uplift modeled as intrusion of a near horizontal magmatic sill at  $\sim 10$  km depth beneath the Yellowstone caldera. One unusual earthquake, the 5 November 2007  $M_w$  3.3 earthquake, occurred in a volume of expected crustal expansion above the inflating magmatic sill. A notable 60% isotropic expansion component was determined for this earthquake with a 3.2 cm opening across an area of 0.12 km<sup>2</sup>. We propose that the inflation of the magmatic sill activates a high-pressurized fluid migration upward which in turn triggers dilatational deformation inducing this earthquake. Another dilatational deformation earthquake, the 9 January 2008  $M_w$  3.8 earthquake, occurred on the northern rim of the caldera. The moment tensor solution for this earthquake shows that the source mechanism had a 30% of the energy associated with tensile dislocation corresponding to a 3.3 cm opening crack over an area of 0.58 km<sup>2</sup>. We suggest that stress changes produced by a collocated  $M_w$  3.4 earthquake may have increased the fracture permeability promoting fluid migration and thus encouraging the dilatational dislocation. These dilatational source earthquakes are the first non–double couple earthquakes to be documented unambiguously in the 35 year recording period of the Yellowstone seismic network.

**Citation:** Taira, T., R. B. Smith, and W.-L. Chang (2010), Seismic evidence for dilatational source deformations accompanying the 2004–2008 Yellowstone accelerated uplift episode, *J. Geophys. Res.*, 115, B02301, doi:10.1029/2008JB006281.

### 1. Introduction

[2] The Yellowstone caldera is one of the world's largest active silicic calderas and is characterized by the 40 km wide by 60 km long caldera formed by the most recent eruption at 0.64 Ma ago [Christiansen, 2001]. Geodetic measurements beginning in 1923 have revealed that the Yellowstone caldera has experienced multiple episodes of caldera-wide deformation of both uplift and subsidence, with deformation rates averaging 1–2 cm/a [Pelton and Smith, 1979; Dzurisin et al., 1994; Wicks et al., 1998, 2006; Puskas et al., 2007; Vasco et al., 2007]. Continuous Global Positioning System (GPS) and Interferometric Synthetic Aperture Radar (InSAR) measurements recently revealed an episode of rapid ground deformation of the caldera beginning in the middle of 2004 with unexpected high rates

of up to  $\sim 7$  cm/a (corresponding to over 20 cm uplift) in the caldera and concomitant subsidence of the Norris Geyser basin area of  $\sim 2$  cm/a [Chang et al., 2007].

[3] The Yellowstone Plateau Volcanic Field [Christiansen, 2001, Figure 1] is one of the most seismically active parts of the 1300 km long Intermountain Seismic Belt extending from Montana to Arizona [Smith and Sbar, 1974; Smith and Arabasz, 1991]. Over 20,000 earthquakes have been located in Yellowstone National Park since 1973 [Husen and Smith, 2004], averaging 1000–3000 earthquakes per year. The largest historic earthquake of the entire Intermountain region was the 1959  $M_S$  7.5 Hebgen Lake earthquake [Doser, 1985] that occurred on the northwest rim of the Yellowstone caldera. The 1975  $M_L$  6.1 Norris Junction earthquake has been the largest inner caldera earthquake in historic time [Pitt et al., 1979].

[4] Seismicity within the Yellowstone caldera is characterized by small shallow earthquakes ( $M < 3$ ) with focal depths generally less than 5 km [Husen and Smith, 2004; Farrell et al., 2009] compared to deeper seismicity of up to  $\sim 20$  km depth outside the caldera. The shallow seismicity is inferred to reflect brittle failure above a crystallizing magma system located  $\sim 6$  to 15 km beneath the caldera that was elucidated by crustal seismic traveltimes tomography [Miller

<sup>1</sup>Department of Geology and Geophysics, University of Utah, Salt Lake City, Utah, USA.

<sup>2</sup>Now at Berkeley Seismological Laboratory, University of California, Berkeley, California, USA.

<sup>3</sup>Now at Department of Earth Sciences, National Central University, Jhongli City, Taiwan.

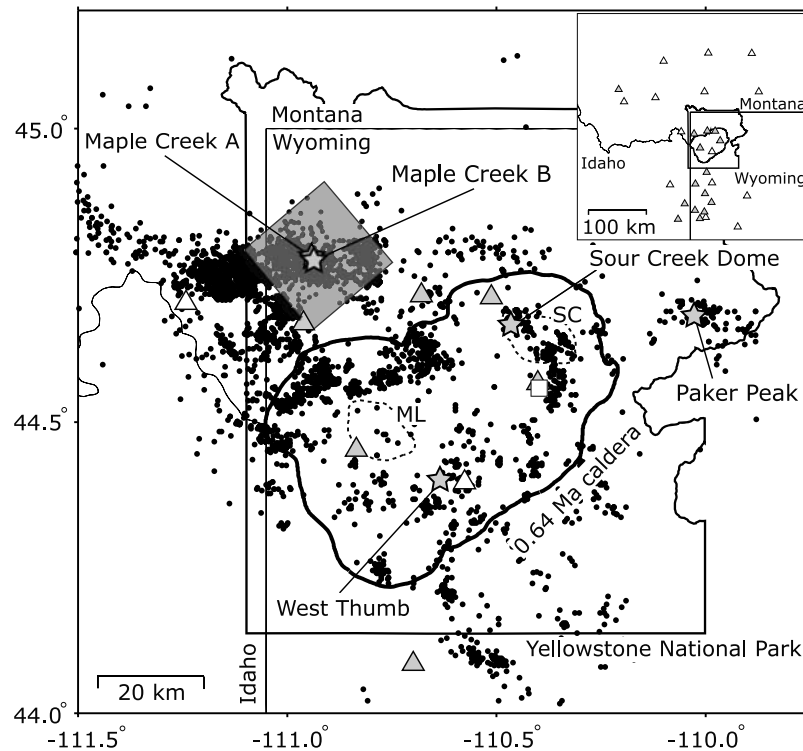


**Figure 1.** Map of Yellowstone National Park showing the locations of broadband seismometers (triangles) and the five  $M \geq 3$  Yellowstone earthquakes (gray stars) examined in this study. Broadband seismometers of the EarthScope Transportable Array and other networks are shown in open and gray triangles, respectively. Dots and open squares are locations of Yellowstone earthquakes during 2003–2008 and the GPS station showing its vertical displacement in Figure 2. Gray square indicates the area of background seismicity used for examining the depth of brittle-ductile transition zone. The 0.64 million year Yellowstone caldera boundary is outlined with a solid line, and the Sour Creek (SC) and Mallard Lake (ML) resurgent domes with dashed lines. Also shown are boundaries of Yellowstone National Park (black line) and state (thin lines). Inset map shows locations of broadband seismometers around Yellowstone National Park (Wyoming, Idaho, and Montana).

and Smith, 1999]. Local seismic tomographic studies imaged this crystallizing magma body as a  $\sim 5\%$  reduction in  $P$  wave velocity with up to  $\sim 15\%$  partial melt [Benz and Smith, 1984; Miller and Smith, 1999; Husen et al., 2004a]. The crystallizing magma is also considered to be responsible for the extraordinarily high heat flow flux of the caldera of  $\sim 2000$  mW/m<sup>2</sup> [Morgan et al., 1977; Fournier, 1989]. Recent teleseismic tomographic studies also reveal north-west dipping low  $P$  (1.0%) and  $S$  (2.5%) wave velocities in the upper mantle from 80 km to at least  $\sim 660$  km depth that have been interpreted as a plume [Yuan and Dueker, 2005; Waite et al., 2006; Smith et al., 2009].

[5] The Yellowstone caldera began to inflate at rates up to 7 cm/a in the middle of 2004 [Chang et al., 2007] and has continued moving upward at similar to slightly lower rates throughout 2008. This uplift episode has been accompanied by a reduction in seismic activity [Chang et al., 2007]. Yet, the physical mechanism of earthquakes in and around the Yellowstone caldera during this period of unusually high deformation is unclear. Yellowstone earthquakes generally result from tectonic and magmatic sources and interactions between these features [e.g., Smith and Sbar, 1974; Waite and Smith, 2002]. For example, Waite and Smith [2002] proposed that a migration of hydrothermal fluids radially outward from the Yellowstone caldera triggered the largest

historic earthquake swarm in Yellowstone National Park, the autumn 1985 earthquake swarm located across the northwest rim of the Yellowstone caldera.

[6] In this study, we use moment tensor inversions to examine the seismic source processes of five well-recorded  $M \geq 3$  Yellowstone earthquakes that occurred during the 2004–2008 accelerated uplift, so as to further evaluate the possibility of magmatic-tectonic interactions during the 2004–2008 unrest at the Yellowstone caldera. By using recently installed high-quality broadband seismometers, we identified two unusual Yellowstone earthquakes that were characterized by significant source volume increases. We propose that pressurized hydrothermal fluids in the upper crustal magma system triggered the two non-double couple earthquakes. Notably they represent the first dilatational source earthquakes reliably recorded in the Yellowstone hydrothermal system.

## 2. Data and Methodology

[7] The seismic data used in this study were recorded by multiple networks of broadband seismometers (Figure 1) operated by the University of Utah, U.S. Geological Survey, and EarthScope's USArray program. The deployment of University of Utah broadband seismometers near the

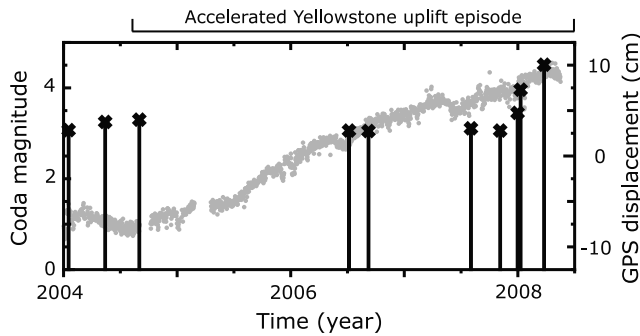


**Figure 2.** Magnitude-time plot for  $M$  3+ Yellowstone earthquakes (crosses) during 2004–2008. Also shown are vertical Yellowstone ground motions (gray circles) observed at Yellowstone Lake, GPS station LKWY shown in Figure 1.

Yellowstone caldera began in 1995, with five broadband seismometers installed by late 2003. USArray deployed 10 broadband seismometers around Yellowstone National Park (Wyoming, Idaho, and Montana) in late 2007. These newly deployed seismometers significantly improved the resolving power of our moment tensor solutions. Ten  $M$  3+ Yellowstone earthquakes were observed in 2004–2008 (Figure 2) where data from at least five broadband seismometers were available. For the first five  $M$  3+ earthquakes, however, only a few broadband seismograms with high signal-to-noise ratio are available. The latter five  $M$  3+ earthquakes (Table 1), however, were well recorded by  $\sim 10$  broadband seismometers with good azimuthal distribution.

[8] The objective of this study was to characterize the source properties of these  $M$  3+ Yellowstone earthquakes to evaluate how earthquake activity may reflect the interaction of the geodetically imaged inflating magma source of the 2004–2008 Yellowstone caldera uplift episode [Chang *et al.*, 2007] with faults and fluid pathways associated with the Yellowstone hydrothermal system. As shown in Figure 1, two of the five  $M$  3+ earthquakes occurred inside the Yellowstone caldera while the others were located 10–20 km from the caldera. To gain insight into the physical mechanisms of the earthquakes, moment tensor inversions with five different source models were performed: (1) shear faulting, (2) shear faulting + CLVD (compensated linear vector dipole), (3) shear faulting + CLVD + isotropic component, (4) shear faulting + isotropic component, and (5) shear faulting + tensile crack (Appendix A). Moment tensor inversions using the first three source models are referred to as double-couple, deviatoric, and full moment tensor inversions, respectively, and have been widely used for examining source processes of earthquakes occurring in the upper crust to the lower mantle [e.g., Lay and Wallace, 1995].

[9] Employing full moment tensor inversions, several studies have identified unusual earthquakes with notable non-double couple (i.e., isotropic) components in volcanic and geothermal areas such as the Geysers, California [e.g., Ross *et al.*, 1996], Hengill-Grensdalur, Iceland [Miller *et al.*, 1998], and the Long Valley caldera, California [e.g., Dreger *et al.*, 2000; Foulger *et al.*, 2004]. The presence of a volumetric component can be a direct evidence for fluid involvement in earthquake source process [Julian and Sipkin, 1985; Kanamori *et al.*, 1993]. For example, Dreger *et al.* [2000] identified four  $M$  4+ earthquakes with 30–40% volumetric components accompanying the unrest at the Long Valley caldera in late 1997–early 1998. During this unrest, an anomalous 10 day compressional strain transient ( $\sim 0.3$  microstrain) was also observed [Hill *et al.*, 2003; Roeloffs *et al.*, 2003]. Dufumier and Rivera [1997], however, showed that spurious volumetric source components may result from trade-offs among tensor elements with poor data quality. In addition, estimating multiple compensating volumetric components requires unphysical or highly complicated earthquake source process. Moreover, full moment tensor decompositions are nonunique [e.g., Julian *et al.*, 1998].

[10] To evaluate the presence of volumetric component, we therefore considered two source models that are shear faulting with an isotropic or tensile crack component, as noted above. Both source models yield volumetric components in the earthquake source process. To compute Green's functions for moment tensor inversions, a three-dimensional finite difference method [Ohminato and Chouet, 1997] was used for the broadband seismic data recorded inside the Yellowstone caldera where inhomogeneous velocity structures with topographic effects should be considered. The grid spacing was set to be 100 m.  $P$  and  $S$  wave velocity and density structures were constrained by the three-dimensional local seismic traveltime tomography [Husen *et al.*, 2004a] and gravity data [DeNosaquo *et al.*, 2009] in the Yellowstone caldera. Values of attenuation were assumed to be 600 and 300 for  $P$  and  $S$  waves, although a  $P$  wave attenuation model has been estimated in the Yellowstone caldera [Clawson *et al.*, 1989] that suggests a high attenuation value ( $\sim 30$ ) in the surface layer within the caldera. However, we found that variations in the attenuation model slightly changed estimated scalar seismic moments but did not change percentages of non-double couple components significantly. The surface topography data was interpolated from available U.S. Geological Survey topographic data. For seismic data recorded outside the caldera, we used a frequency wave number method [Bouchon and Aki, 1977]. We used the one-dimensional velocity model (Table 2) that is used for routinely determining Yellowstone earthquake locations by the University of Utah Seismograph Stations. The attenuation model was the same as for the inside of the caldera.

**Table 1.** Five  $M$  3+ Yellowstone Earthquakes Examined in This Study

Earthquake	Date	Origin Time (UTC)	Latitude ( $^{\circ}$ N)	Longitude ( $^{\circ}$ E)	Depth (km)	Local Magnitude
Sour Creek Dome	2007/08/03	06:25:35.47	44.660	-110.463	4.0	3.1
West Thumb	2007/11/05	05:43:54.22	44.406	-110.615	4.0	3.1
Maple Creek A	2007/12/31	03:29:20.78	44.778	-110.940	9.9	3.6
Maple Creek B	2008/01/09	21:37:36.97	44.776	-110.937	9.3	3.7
Parker Peak	2008/03/25	11:59:36.91	44.680	-110.041	4.9	4.1

**Table 2.** Velocity, Density, and Attenuation Structures Used for Calculating Green's Functions for Broadband Seismometers Outside the Yellowstone Caldera

Thickness (km)	<i>P</i> Wave Velocity (km/s)	<i>S</i> Wave Velocity (km/s)	Density (kg/m <sup>3</sup> )	Attenuation of <i>P</i> Wave	Attenuation of <i>S</i> Wave
1.9	3.90	2.30	2.50	600	300
6.1	5.67	3.37	2.50	600	300
13.0	6.02	3.59	2.67	600	300
19.0	6.70	3.94	3.00	600	300
40.0	7.90	4.62	3.30	600	300

[11] The locations of the five  $M \geq 3$  Yellowstone earthquakes were well determined by the probabilistic earthquake location algorithm NonLinLoc [Lomax *et al.*, 2001] and the three-dimensional seismic velocity model of Husen *et al.* [2004a]. The uncertainties (standard deviation) in locations of the earthquakes in this study are less than 0.4 km and 1.0 km in horizontal and in vertical directions, respectively, except for a vertical uncertainty of 3 km for the 3 August 2007  $M_w$  3.1 Sour Creek Dome earthquake. To compute Green's functions, the source locations were fixed.

[12] We first applied a deviatoric moment tensor inversion [Dreger *et al.*, 2000] for the five earthquakes and calculated their variance reductions (VR) for individual stations defined as [e.g., Templeton and Dreger, 2006]

$$\text{VR} = \left(1 - \frac{\sum_{t=1}^T (u^o(t) - u^s(t))^2}{\sum_{t=1}^T (u^o(t))^2}\right) \times 100, \quad (1)$$

where  $u^o(t)$  and  $u^s(t)$  are observed and synthetic data at the  $t$ th data point and  $T$  is the total number of samples. A variance reduction of 100% indicates a perfect fit of the observed data to synthetic data. We did not use seismic data from earthquake station pairs with negative VR for further analysis. Evaluated negative values of VR appear to be due to low signal-to-noise levels for those seismic data.

[13] Band-pass filterers were initially set to be 10–50 s and 5–15 s periods for Nanometrics (Trillium 240) and Güralp (CMG-40T and CMG-3ESP) instruments, respectively, based on their limitations of long-period response. These passbands are similar to those for previous studies that successfully estimated moment tensor components for  $M \geq 4$  earthquakes [e.g., Dreger *et al.*, 2000]. We then slightly modified passbands for individual station-earthquake pairs so that the average VR values were maximized. We note that estimated moment tensor components did not significantly change due to the choice of passbands. The time window lengths were set to be 128 s and 60 s for seismograms of  $M \geq 4$  and  $M < 4$  earthquakes, respectively, and a 30 s time window length was used for seismograms band-pass filtered between 5 s and 15 s. Following Ford *et al.* [2009], the maximum value of time shift for synthetic data was set to be 3 s. This maximum value would be expected to correct errors in earthquake locations and uncertainties in velocity models and also avoid phase cycle skips.

### 3. Results

[14] We examined source mechanisms for the five  $M \geq 3$  Yellowstone earthquakes listed in Table 1 by using five different source models described above. We used a linear

inversion procedure from Dreger *et al.* [2000] for deviatoric and full moment tensor inversions, and a grid search approach for other three source models (shear faulting, shear faulting + isotropic component, and shear faulting + tensile crack) because the estimations in moment tensor solution for these models are a nonlinear problem [Minson *et al.*, 2007]. The grid search tested all possible combinations for strike, dip, and rake in increments of five degrees, for double-couple and total (e.g., double-couple + tensile crack components) scalar seismic moments in increments of 0.1 seismic moment magnitude ( $M_w$ ), and for percentage of isotropic and tensile crack seismic moments in increments of 10% of total scalar seismic moment.

[15] We used  $F$  test statistics to assess the statistical significance of CLVD, isotropic, and tensile crack components, with the double-couple moment tensor solution as reference [Dreger *et al.*, 2000; Templeton and Dreger, 2006]. As similar to Templeton and Dreger [2006], the variance for the  $F$  test statistics can be expressed as

$$s^2 = \sum_{i=1}^N \left( \frac{\sum_{t=1}^T (u_i^o(t) - u_i^s(t))^2}{(K_i - M)} \right), \quad (2)$$

where  $K_i$  is the uncorrelated data point for the  $i$ th station,  $M$  is the model parameter, and  $N$  is the number of analyzed stations.  $K$  can be formed from  $K = 2f_h T_w$  where  $f_h$  and  $T_w$  are a band-pass high corner in hertz and a time window length, respectively [e.g., Silver and Chan, 1991]. For the double-couple moment tensor inversion, the model parameter is four (strike, dip, rake, and double-couple moment) while  $M = 5$  for source modes constituting of shear faulting + one non-double couple component and  $M = 6$  for the full moment tensor inversion. The  $F$  test statistic is defined as the ratio of the variances comparing the double-couple solution,  $s_{\text{DC}}^2$ , to other variances,  $s^2$ ; that is  $F = s_{\text{DC}}^2/s^2$ . Given the degrees of freedom  $\nu = \bar{K} - M - 1$  [Menke, 1989], where  $\bar{K}$  is the sum of uncorrelated data points for analyzed stations, confidence levels for the  $F$  test statistics were estimated. We used the 90% confidence level to identify non-double couple components such as tensile cracks [e.g., Dreger *et al.*, 2000]. If the largest  $F$  test statistic value fell below the 90% confidence level, then we assigned the double-couple source model to be the best fitting source model. We evaluated uncertainties in estimated parameters (e.g., percentage of non-double couple components and principal stress directions) by using a bootstrap technique [Efron and Tibshirani, 1993] with 1000 subsample data sets.

[16] As shown in Table 3, we found that two of five  $M \geq 3$  Yellowstone earthquakes had statistically significant volumetric components (i.e., shear faulting + isotropic

**Table 3.** Results of  $F$  Test Statistics for Five Different Source Models and Moment Tensor Solutions for Best Fitting Source Models<sup>a</sup>

Earthquake	$F_{CLVD}$	$F_I$	$F_{TC}$	$F_F$	$F_{90}$	$M_0$ ( $10^{14}$ N m)	$M_w$	VR (%)	Best Fitting Source Model
Sour Creek Dome	1.00	1.05	1.03	1.01	1.37	0.56	3.1 ( $\pm 0.14$ ) <sup>b</sup>	37	Shear faulting
West Thumb	1.00	1.37 (1.30–1.51) <sup>c</sup>	1.34	1.33	1.29	1.11	3.3 ( $\pm 0.06$ ) <sup>b</sup>	33	Shear faulting + isotropic
Maple Creek A	1.02	1.07	1.08	1.03	1.27	1.57	3.4 ( $\pm 0.09$ ) <sup>b</sup>	46	Shear faulting
Maple Creek B	1.15	1.30	1.54 (1.33–1.82) <sup>c</sup>	1.50	1.23	6.24	3.8 ( $\pm 0.07$ ) <sup>b</sup>	65	Shear faulting + tensile crack
Parker Peak	1.00	1.01	1.01	1.14	1.25	24.83	4.2 ( $\pm 0.04$ ) <sup>b</sup>	68	Shear faulting

<sup>a</sup> $F_{CLVD}$ ,  $F_I$ ,  $F_{TC}$ , and  $F_F$  are  $F$  test statistics comparing the shear-faulting source model to shear-faulting + CLVD, shear-faulting + isotropic, shear-faulting + tensile crack, and shear-faulting + CLVD + isotropic source models, respectively.  $F_{90}$  is the threshold value of  $F$  test statistic for the 90% confidence level and is determined based on the number of available stations and applied band-pass filters. Seismic moment ( $M_0$ ), moment magnitude ( $M_w$ ), and variance reduction (VR) were estimated by using the best fitting source model.

<sup>b</sup>Standard deviations are determined by using bootstrap approaches.  
<sup>c</sup>Confidence intervals of 90% are evaluated by using jackknife tests.

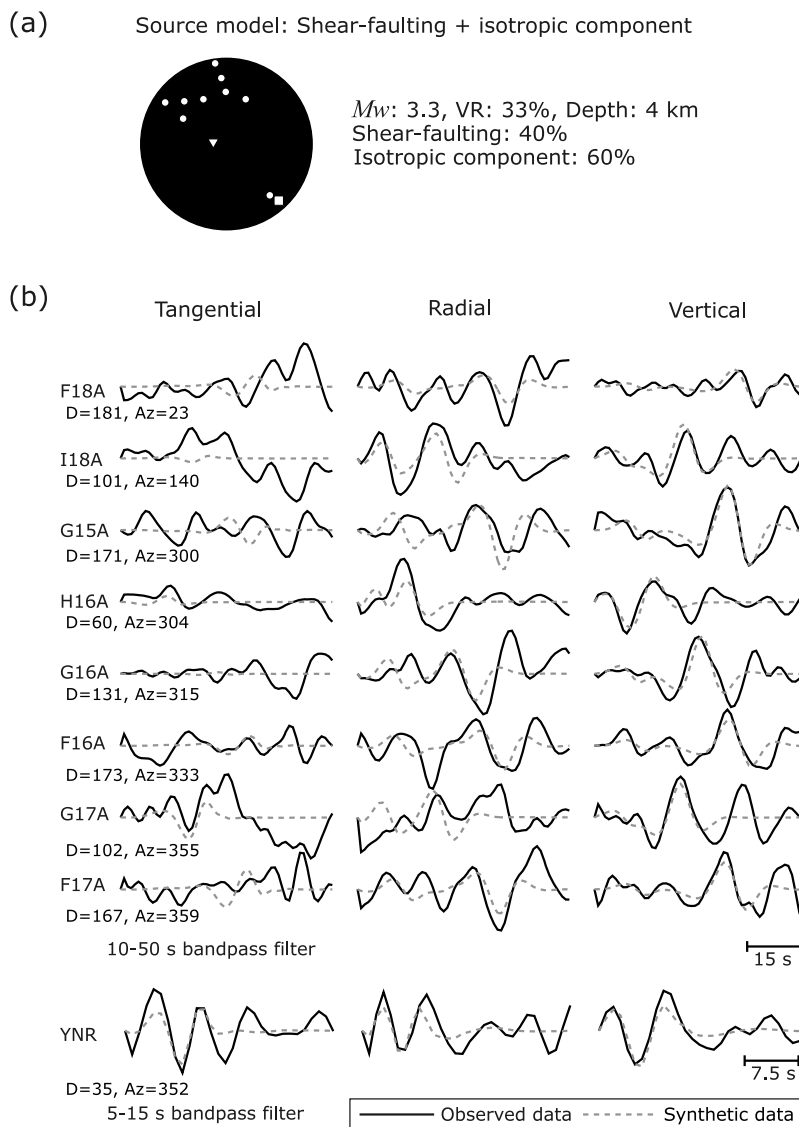


**Figure 3.** Results of moment tensor inversion for the West Thumb earthquake employing shear faulting + isotropic component source model. (a) The best fitting source mechanism with the used broadband seismometers (circles). Reverse triangle and square are P and T axes, respectively. (b) Observed (black lines) and synthetic (dashed gray lines) data based on the best fitting source mechanism. Also shown are earthquake station distances (D) in km and azimuths (Az) in degree from north.

**Table 4.** Percentages of Volumetric Components, Changes in Source Volume, Fault Area, and Opening Dislocation<sup>a</sup>

Earthquake	Volumetric Component (%)	Volume Change (m <sup>3</sup> )	Fault Area (km <sup>2</sup> )	Opening Dislocation (cm)
West Thumb	60	$4.0 \times 10^3$	0.12	3.2
Maple Creek B	30	$18.7 \times 10^3$	0.58	3.3

<sup>a</sup>Shear faulting + isotropic component and shear faulting + tensile crack source models were used for the West Thumb and the Maple Creek B earthquakes, respectively.

component or shear faulting + tensile crack). One of the  $M$  3+ earthquakes with a notable volumetric component was the 5 November 2007 West Thumb earthquake (Figure 3). A shear faulting + isotropic component source model is the best fitting source mechanism for the West Thumb earthquake (Table 3). The value of  $F$  test statistic for the best fitting source model is 1.37, which is the almost same as the 95% confidence level,  $F_{95} = 1.38$ . Our moment tensor analysis suggests that the volumetric component of the West Thumb earthquake can be characterized by an isotropic component rather than tensile crack, although the reduction in variance for a shear faulting + tensile crack source model is statistically significant above 90% level. We estimate a 60% volumetric expansion component with a standard deviation of  $\pm 16\%$ . The scalar seismic moment ( $M_0$ ) is estimated to be  $1.11 \times 10^{14}$  N m ( $M_w = 3.3$ ). Using the scalar seismic moment of isotropic component  $M_I$ , a change in source volume  $\Delta V$  can be determined from the equation  $M_I = [\lambda + (2/3)\mu]\Delta V$ , where  $\lambda$  and  $\mu$  are the Lamé constants [Aki and Richards, 1980]. As similar to Gottsmann *et al.* [2006] and Jónsson [2009], we assumed  $\lambda$  and  $\mu$  to be 10 GPa throughout this study. The estimated value of  $\Delta V$  for the West Thumb earthquake is  $4.0 \times 10^3$  m<sup>3</sup> (Table 4).

[17] The VR of the best fitting model for the West Thumb earthquake is 33% (Table 3), which is relatively low compared with those for previous studies [e.g., Minson *et al.*, 2007]. However, previous studies have modeled source mechanisms for mainly  $M_w > 5$  moderate earthquakes with higher signal-to-noise ratios than we found for the  $M_w$  3.3 West Thumb earthquake in the 10–50 s period range.

[18] We thus further tested the stability of our moment tensor solution by using a jackknife test [e.g., Efron, 1982] to access the possibility that the determined isotropic component is due to specific stations [e.g., Dreger *et al.*, 2000; Ichinose *et al.*, 2003; Templeton and Dreger, 2006]. We performed the jackknife test which involved repeating moment tensor inversions with two different source models: (1) shear faulting and (2) shear faulting + isotropic component, by using 6 station subsets obtained by deleting 3 stations (corresponding to one-third of the total number of stations) and calculated the values of  $F$  test statistic for individual subsets. We considered the subsets with VR higher than 30% for their preferred source models (i.e., shear faulting or shear faulting + isotropic component source model) that yield the highest VR, in order to suppress apparent non-double couple components due to poor data quality [Dufumier and Rivera, 1997], which we seek to avoid. Our jackknife test shows that the  $F$  test statistic value ranges from 1.30 to 1.51 for the 90% confidence interval and indicates that the lower bound is larger than the 90% confidence level,  $F_{90} = 1.29$  that was used to identify non-double couple component for the West Thumb earthquake.

[19] We additionally noted that all reliable first  $P$  waves observed at over 20 stations (both short-period and broadband seismometers around the Yellowstone caldera) have clear compressional first motions (Figure 4a), which is consistent with predicted first motions from the best fitting source model (shear faulting + isotropic component) determined by our moment tensor inversion (Figure 3a). With the good station azimuthal coverage, the first motion data suggests that a double-couple source mechanism is not valid for the West Thumb earthquake (Figure 4a). Errors in earthquake location will, however, introduce spurious non-double couple source mechanisms. We examined the sensitivity of focal mechanisms to changes in focal depth because the estimation in focal mechanisms will be more sensitive to focal depths rather than lateral variations in earthquake location [e.g., Hardebeck and Shearer, 2002]. We considered two possible focal depths: (1) 3 km and (2) 5 km that are perturbed from the relocated earthquake location (Table 1). These two values approximately correspond to the one-sigma confidence intervals of the focal

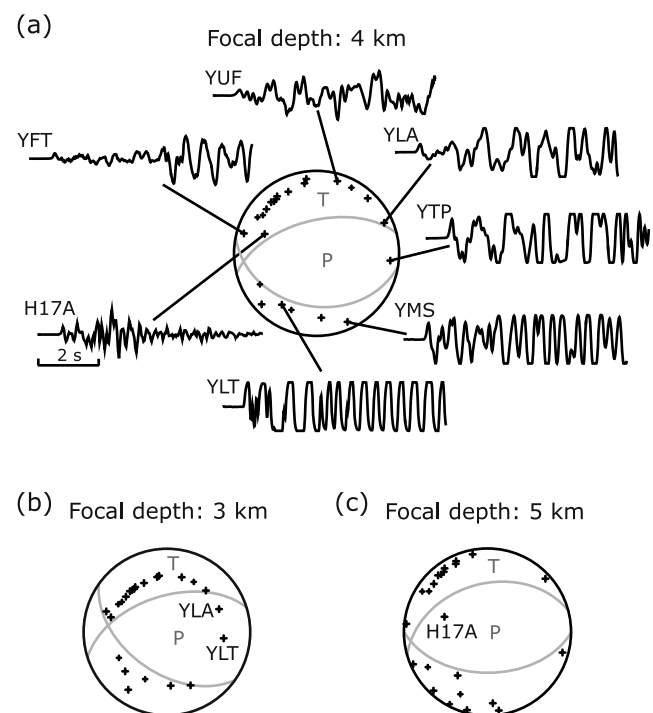


**Figure 4.** Focal mechanism solutions for the West Thumb earthquake with three different focal depths: (a) 4 km, (b) 3 km, and (c) 5 km, by using  $P$  wave polarities. Compressional first motions (crosses) are observed at all of stations where reliable first motions are observed. Gray lines in the focal spheres are preferred fault planes assuming a double-couple source model. Also shown are examples of observed waveforms in Figure 4a.

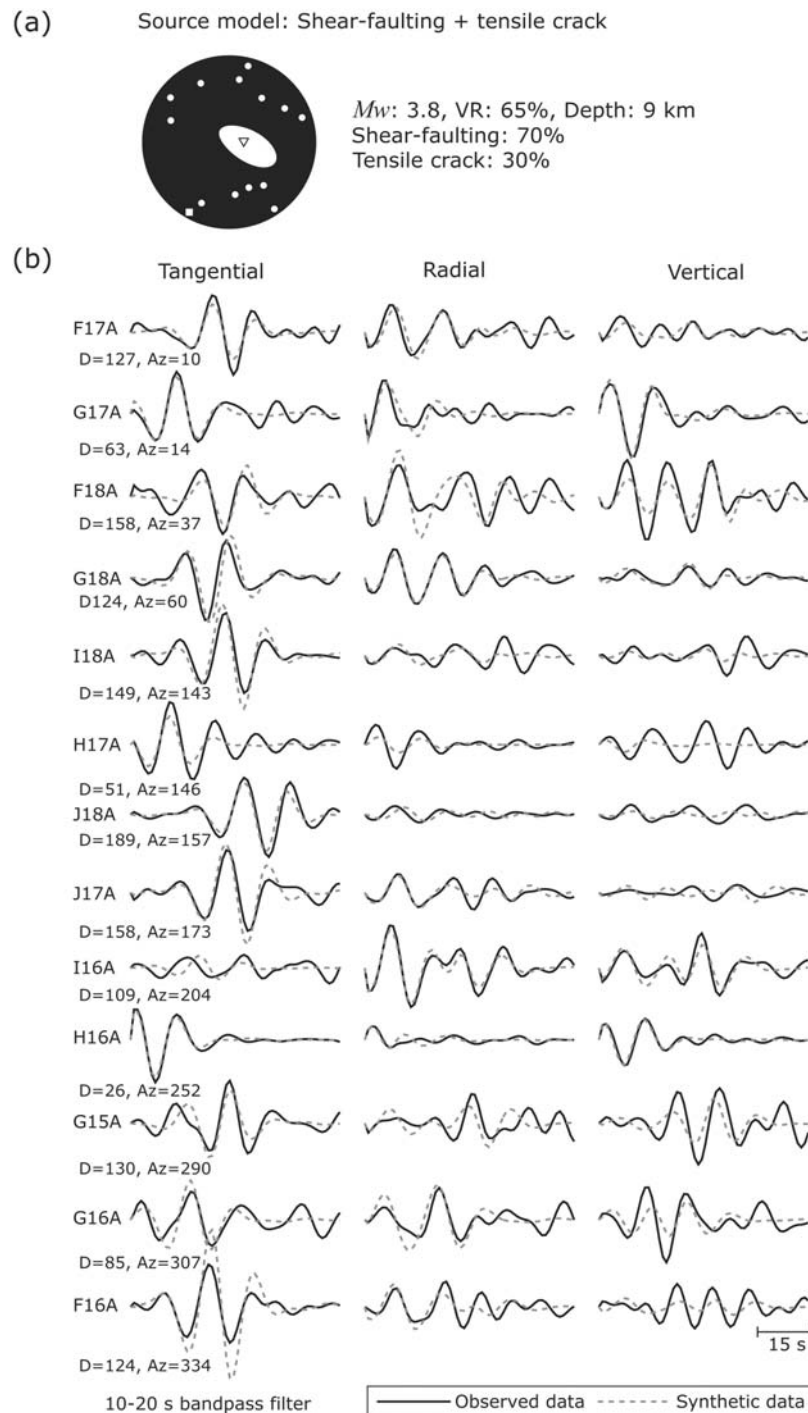


**Figure 5.** Same as Figure 3 except for the Maple Creek B earthquake employing shear faulting + tensile crack source model.

depth (4 km) for the West Thumb earthquake. We found that neither the shallow or deep focal depth solution is consistent with double-couple source mechanisms (Figures 4b and 4c), which supports the non-double couple source model (i.e., shear faulting + isotropic component) inferred from our moment tensor inversion.

[20] The other earthquake with a significant volumetric component occurred on 9 January 2008 referred to here as the Maple Creek B earthquake, located in the northern caldera rim area (Figure 5). For this earthquake, a shear

faulting + tensile crack is the best fitting source model (Table 3). The best fitting source model satisfies the  $F$  test statistic for significance above 99% level,  $F_{99} = 1.47$ . As similar to the West Thumb earthquake, we assessed the stability of the moment tensor solution by using a jackknife test with 9 station subsets where 4 stations (approximately one-third of the total station number) are deleted. The jackknife test revealed the value of  $F$  statistic ranging from 1.33 through 1.82 for the 90% confidence interval. The calculated lower bound is larger than the 90% confidence

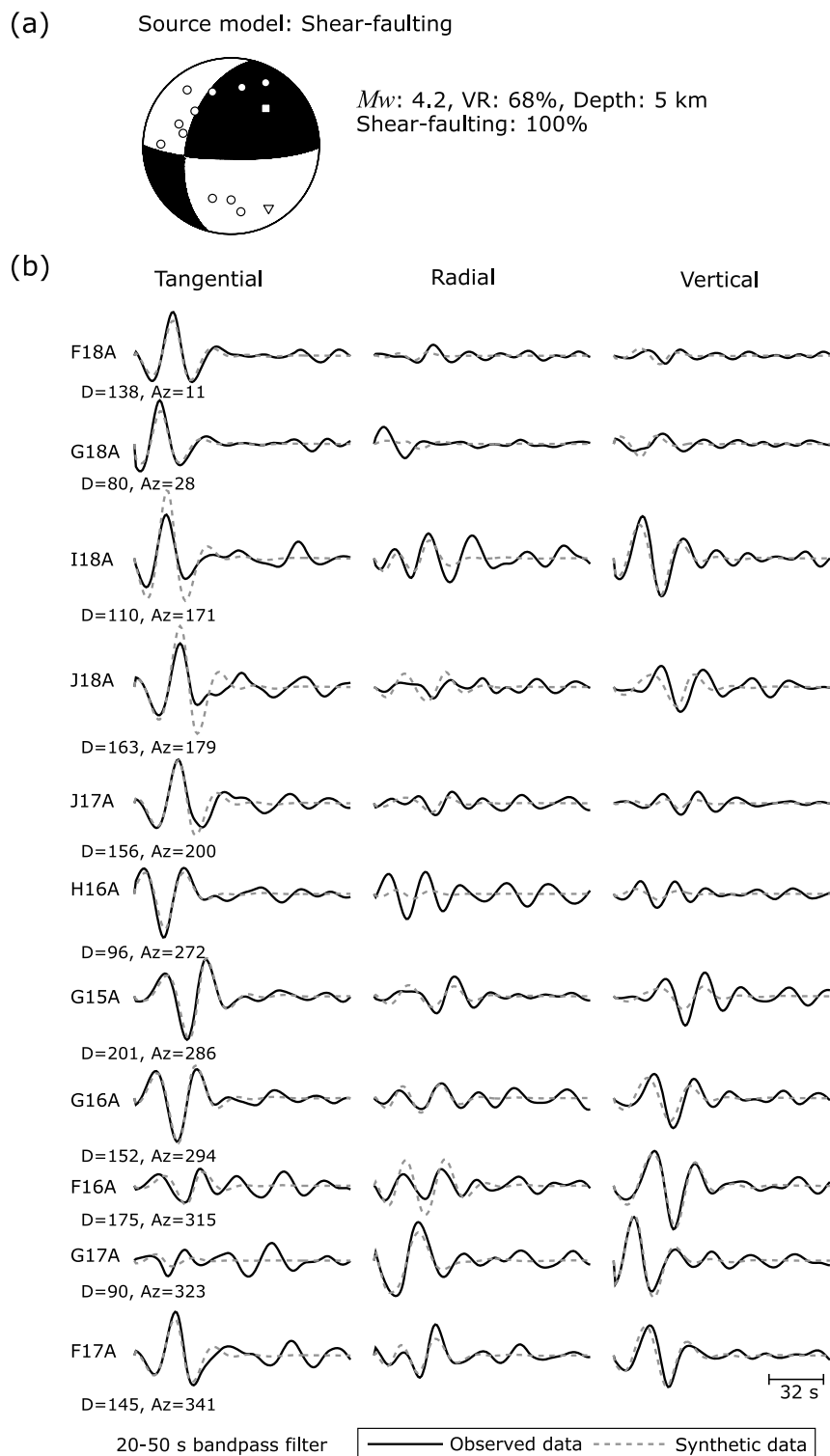


**Figure 6.** Same as Figure 3 except for the Parker Peak earthquake employing shear faulting source model.

level,  $F_{90} = 1.23$  that was used to detect non-double couple component for the Maple Creek B earthquake. We found a 30% (with a standard deviation of  $\pm 8\%$ ) opening crack component for the Maple Creek B earthquake with a total the estimated seismic moment of  $6.24 \times 10^{14}$  N m ( $M_w$  3.8). The volumetric change associated with the Maple Creek B earthquake can be determined through the equation  $M_{TC} = \lambda \Delta V$ , where  $M_{TC}$  is the scalar seismic

moment of the tensile crack component, assuming a Poisson solid (i.e.,  $\lambda = \mu$ ) [e.g., *Chouet, 1996*]. Assuming  $\lambda = 10$  GPa, the estimated value of  $\Delta V$  for this earthquake is  $18.7 \times 10^3$  m<sup>3</sup> (Table 4).

[21] We found that the remaining three  $M \geq 3$  Yellowstone earthquakes could be fitted by source models with non-double couple components, but these did not satisfy  $F$  test statistics for significance above the 90% level (Table 3).

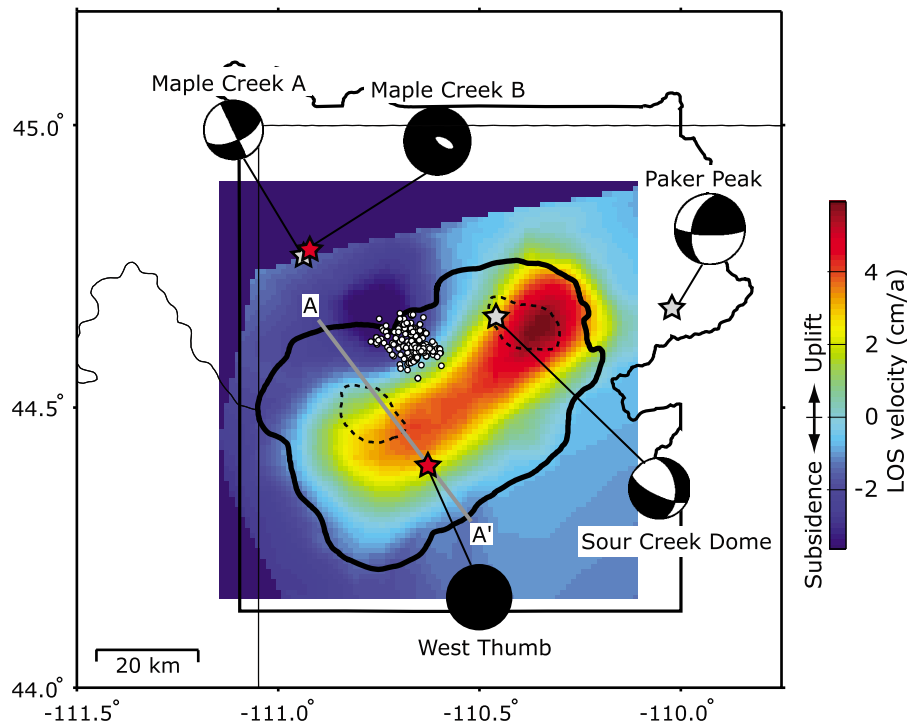


**Figure 7.** Observed Yellowstone accelerated uplift and subsidence during 2004–2006 inferred from the GPS and InSAR data [Chang *et al.*, 2007]. Colors indicate interpolated the satellite line-of-sight (LOS) velocity. Also shown are the estimated best fitting source mechanisms of the  $M$  3+ Yellowstone earthquakes that we examined. Red and gray stars indicate earthquakes accompanying dilatational dislocations and tectonic earthquakes (i.e., pure shear dislocation), respectively. White circles are the locations of microearthquakes that have been interpreted as triggered earthquakes by the inflation of the magmatic sill accompanying the 2004–2008 Yellowstone uplift episode [Chang *et al.*, 2007].

Therefore we interpret these three earthquakes to be typical tectonic earthquakes. For example, our moment tensor inversion with shear faulting with one volumetric component source model yields a pure double-couple solution for the 25 March 2008  $M_w$  4.2 Parker Peak earthquake, which strongly suggested that the Parker Peak earthquake resulted in shear faulting process. Indeed, a shear-faulting source model explains the observed data well (Figure 6). Another important result is that CLVD components are unnecessary for source mechanisms of all five  $M$  3+ Yellowstone earthquakes that we examined.

#### 4. Discussion

[22] Using broadband seismic data, we evaluated earthquake source processes for five  $M$  3+ Yellowstone earthquakes occurring in the 2004–2008 Yellowstone accelerated uplift episode (Figure 7). As listed in Table 3, our moment

tensor analysis shows that the source mechanisms for two of these earthquakes are characterized by significant volumetric components. Principal stress directions for the five  $M$  3+ Yellowstone earthquakes examined in this study were extrapolated from their best fitting source models (Table 5). The uncertainties (one sigma) in principal stress directions range from 5 to 30 degrees for the five Yellowstone earthquakes. A similar northeast-southwest direction of T axis (the maximum extensional stress) was estimated for the Maple Creek A and B earthquakes. The estimated T axis directions for the five  $M$  3+ Yellowstone earthquakes are generally consistent with those for background Yellowstone seismicity inferred from first-motion focal mechanisms [Waite and Smith, 2004]. Additionally, the T axis directions determined from the moment tensor inversions appear to follow the long-term strain rotation induced by regional tectonics [e.g., Zoback and Zoback, 1989; Christiansen, 2001] that is northeast-southwest direction in the north rim

**Table 5.** Principal Stress Axes With Their Eigenvalues for the Best Fitting Source Models<sup>a</sup>

Earthquake	T Axis			I Axis			P Axis		
	Value	Trend	Plunge	Value	Trend	Plunge	Value	Trend	Plunge
Sour Creek Dome	0.6	229.6	13.1	0	131.5	31.3	-0.6	339.3	55.5
West Thumb	1.1	137.1	9.5	0.7	45.8	8.2	0.2	275.6	77.4
Maple Creek A	1.6	21.6	14.1	0	143.3	64.5	-1.6	286.1	20.8
Maple Creek B	8.8	209.1	6.6	3.5	300.6	12.7	-1.8	92.3	75.7
Parker Peak	24.8	41.3	42.1	0	257.8	41.6	-24.8	149.7	19.2

<sup>a</sup>Extension is positive for stresses. Eigenvalues are given in  $10^{14}$  N m. Trends and plunges are given in degrees clockwise from north and degrees below horizontal, respectively.

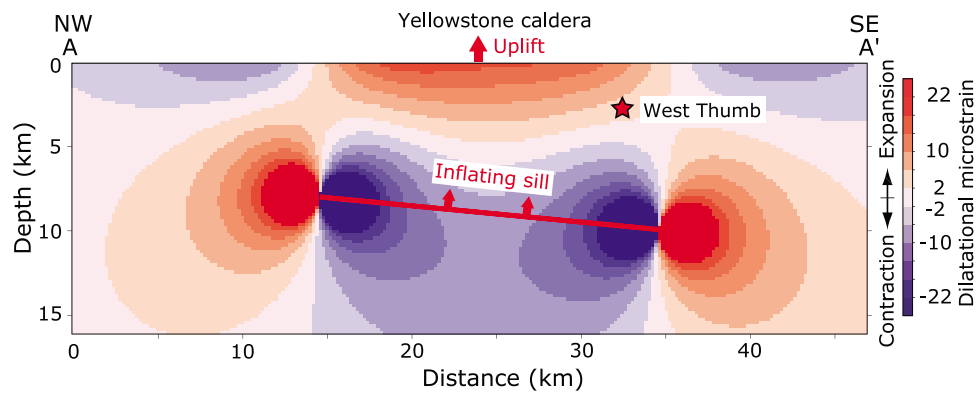


**Figure 8.** Vertical cross section of expected dilatational changes from the GPS-InSAR imaged inflation of the magmatic sill accompanying the 2004–2008 Yellowstone accelerated uplift episode [Chang *et al.*, 2007] along the profiles of A–A' in Figure 7. Red star is the hypocenter of the West Thumb earthquake.

of the Yellowstone caldera (i.e., the Maple Creek A and B earthquakes) to east-west direction in the central part of the caldera (i.e., the Sour Creek Dome and West Thumb earthquakes). Regardless of the presence of coseismic volumetric changes, the fault slip directions for the  $M$  3+ Yellowstone earthquakes in this study seem to be controlled by regional tectonic processes rather than local hydrothermal processes.

[23] One of the unusual earthquakes with a notable volumetric component is the 5 November 2007  $M_w$  3.3 West Thumb earthquake whose volumetric change is estimated to be 60%. The amount of volumetric component is similar to one for a  $M_w$  5.3 earthquake that has been hypothesized to be related to the eruption process of Miyakejima, Japan, 2000 [Minson *et al.*, 2007]. The best fitting source model for the West Thumb earthquake is a shear faulting + isotropic component; it is therefore possible to estimate the size of the opening dislocation  $D_{\perp}$ , across the fault area by utilizing scalar seismic moments of shear dislocation and isotropic component. The characteristic rupture dimension  $\tilde{L}$  can be expressed as [e.g., Lay and Wallace, 1995]

$$\tilde{L} \approx (M_{DC}/\Delta\sigma)^{1/3}, \quad (3)$$

where  $M_{DC}$  and  $\Delta\sigma$  are a scalar seismic moment of double-couple component and a static stress drop, respectively. Following Prejean and Ellsworth [2001] and Ide *et al.* [2003], we assumed  $\Delta\sigma$  to be 1 MPa throughout this study. The estimated value of  $\tilde{L}$  is  $\sim 350$  m and  $D_{\perp}$  is then evaluated to be 3.2 cm based on the equation,  $D_{\perp} = \Delta V/\tilde{L}^2$  [Dreger *et al.*, 2000] given a change in source volume ( $\Delta V$ ) of  $4.0 \times 10^3$  m<sup>3</sup> (Table 4), and the fault area ( $\tilde{L}^2$ ) is calculated to be 0.12 km<sup>2</sup> for the West Thumb earthquake.

[24] The West Thumb earthquake was located on the south side of the deformation area accompanying the 2004–2008 Yellowstone uplift episode and was also close to the West Thumb Geyser basin (Figure 7). The observed rapid deformation signals measured by GPS and InSAR were modeled as an inflating 60 km by 35 km sill located at a depth of 10 km beneath the Yellowstone caldera [Chang *et al.*, 2007] and coincident with the top of the tomographically imaged crustal magma chamber proposed by Husen *et al.* [2004a]. Geochemical studies indicated that hydrothermal reservoirs may exist around the focal depth (4 km) of

the West Thumb earthquake [Fournier, 1989]. Such hydrothermal reservoirs were also proposed to exist beneath the West Thumb Geyser basin, from seismological observations of remotely triggered earthquakes in the basin by the 3 November 2002  $M_w$  7.9 Denali earthquake [Husen *et al.*, 2004b]. The volumetric change associated with the West Thumb earthquake may indicate that this seismic event is related to migration of subsurface pressurized hydrothermal fluid. Geodetic data indicate that a volume increase occurred in the West Thumb source area during the 2004–2008 Yellowstone caldera-wide uplift episode [Chang *et al.*, 2007]. Chang *et al.* [2007] showed that a 10 micro dilatational strain change would have been produced in the earthquake source region by the inflation of the magmatic sill inferred from GPS and InSAR measurements (Figure 8). Given the earthquake location and the expected dilatational change, we propose that a pressurized hydrothermal fluid activated by the magmatic sill induced the occurrence of the West Thumb earthquake. In other words, the West Thumb earthquake may have resulted from the interaction of magma with hydrothermal fluid. A plausible physical model can be described as follows: upwelling magma will heat surrounding hydrothermal fluids; pressures of hydrothermal fluids will be increased; and finally, the increased pressures will exceed the failure strength of the surrounding rocks. Such a mechanism would yield hydrofracturing-type failure with coseismic volumetric change.

[25] On the north side of the deformation area (near Mary Lake,  $\sim 10$  km north of the West Thumb earthquake), a cluster of microearthquakes ( $M < 3$ ) in 2004–2007 (Figure 7) was interpreted to be a set of earthquakes triggered by the inflating magmatic sill accompanying the 2004–2008 Yellowstone uplift episode [Chang *et al.*, 2007]. The source region of these earthquakes is also located in a predicted high dilatational deformation area revealed by geodetic measurements in 2004–2008 as well as near the crystallizing magmatic reservoir inferred from the seismic tomographic imaging [Husen *et al.*, 2004a]. Given a similar physical model of the West Thumb earthquake, some of the triggered earthquakes may have had dilatational components in their earthquake source processes. We were, however, not able to estimate moment tensor solutions for the microearthquakes due to their small magnitudes.

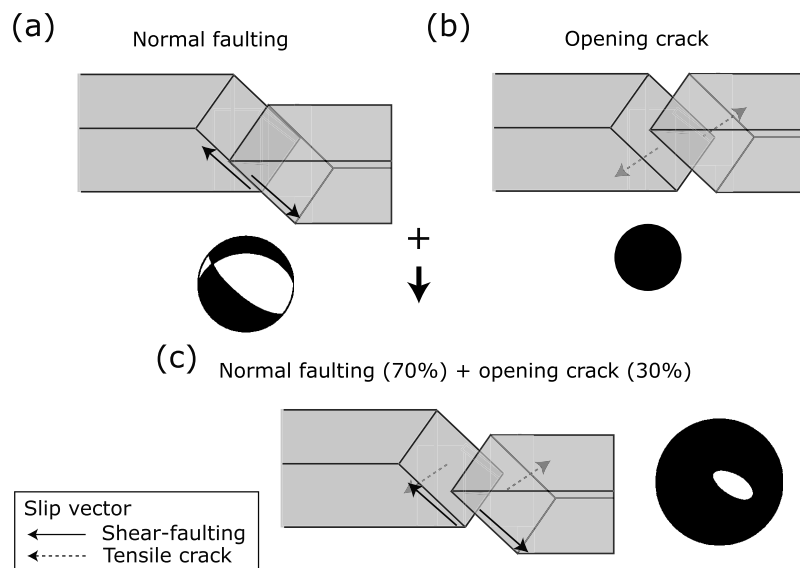


**Figure 9.** Schematic views of the modeled source mechanism of the Maple Creek B earthquake. (a) Normal faulting, (b) opening tensile crack, and (c) the best fitting source model combining normal faulting and opening tensile crack with their expected focal mechanisms. Solid and broken arrows are slip vectors for shear failure and opening tensile components, respectively.

[26] Similar to the West Thumb earthquake, the estimated 30% of opening crack component for the 9 January 2008  $M_w$  3.8 Maple Creek B earthquake suggests pressurization of a fluid-saturated fault [e.g., Dreger *et al.*, 2000]. The estimated source mechanism for the Maple Creek B earthquake is 70% of normal faulting (dip of 65 degrees) and 30% opening tensile crack (Figure 9). For a shear faulting + tensile crack source model, a fault slips with one shear and one tensile dislocations (Appendix A). We are therefore able to estimate the value of tensile dislocation (i.e., slip normal to the shear plane) by making use of scalar seismic moments of shear and tensile dislocations. Using equation (3), the characteristic rupture dimension  $\tilde{L}$ , was estimated to be 760 m with a static stress drop of 1 MPa. Given  $\mu = 10$  GPa, the slip parallel to the fault plane  $D_{//}$ , is then evaluated to be 7.6 cm, through the equation,  $M_{DC} = \mu \tilde{L}^2 D_{//}$  (equation (A7) in Appendix A). The opening dislocation (tensile displacement)  $D_{\perp}$ , is estimated to be 3.3 cm based on  $M_{TC} = \lambda \tilde{L}^2 D_{\perp}$  (equation (A8) in Appendix A), assuming  $\lambda = 10$  GPa. Our moment tensor inversion indicates a 3.3 cm opening tensile dislocation over the fault area ( $\tilde{L}^2$ ) of 0.58 km<sup>2</sup> accompanying the Maple Creek B earthquake (Table 4).

[27] The Maple Creek B earthquake occurred in a sequence of over 150 earthquakes with  $M > 1$  that occurred over approximately three weeks from 25 December 2007 through 15 January 2008 (Figure 10), with most earthquake occurring in a 2 km radius volume. The 31 December 2007  $M_w$  3.4 earthquake, named the Maple Creek A earthquake, occurred a week before the Maple Creek B earthquake. As shown in Table 3, the best fitting source model for the Maple Creek A earthquake is determined to be purely shear faulting (i.e., tectonic earthquake), in contrast to the shear faulting + tensile crack source model for the Maple Creek B earthquake. Both earthquakes appear to have a northerly

striking nodal plane based on the northwest-southeast alignment of the seismicity of the earthquake sequence (Figure 11a).

[28] Focal mechanisms for 11 other  $M \geq 2$  earthquakes in this earthquake sequence were determined from  $P$  wave first motions (Figure 10) using the computer program HASH [Hardebeck and Shearer, 2002] where a double-couple source model is assumed. The source mechanisms of the latter eight  $M \geq 2$  are similar to the estimated double-couple component of the Maple Creek B earthquake. Given this similarity, these eight earthquakes could have a similar volumetric component (opening crack) to that was identified in the source mechanism of the Maple Creek B earthquake.

[29] The estimated focal depths of the Maple Creek A and B earthquakes are 9.9 km and 9.3 km, respectively (Figure 11b). These focal depths are relatively deeper than those for background seismicity ( $\sim 5$  km focal depth) in and around the Yellowstone caldera [Husen and Smith, 2004]. We estimated the depth of the brittle-ductile transition using focal depths of background seismicity. We determined the transition depth by two thresholds: the depth above which 80%,  $h_{80\%}$  and 95%,  $h_{95\%}$ , of earthquakes occur.  $h_{80\%}$  has been used for estimating the transition depth for around the Yellowstone caldera [Smith and Bruhn, 1984] while  $h_{95\%}$  for active fault zones [e.g., Rolandone *et al.*, 2004]. We estimated the depths of  $h_{80\%}$  and  $h_{95\%}$  from  $\sim 2000$  earthquakes that occurred during 2003–2008 in a 20 km x 20 km area (Figure 1) centered on the epicenter of the Maple Creek B earthquake. The estimated depths of the brittle-ductile transition are 8.7 km and 9.4 km for  $h_{80\%}$  and  $h_{95\%}$ , respectively (Figure 11b), after applying an earthquake relocation procedure similar to those for the analyzed  $M \geq 3$  Yellowstone earthquakes. Given these depths, the focal depths of the Maple Creek A and B earthquakes appear to

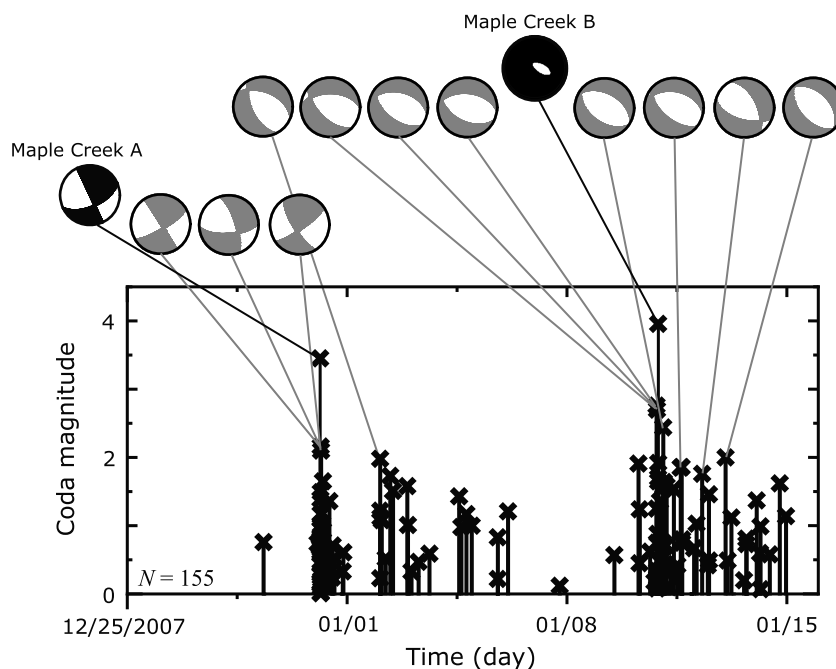


**Figure 10.** Magnitude-time plot for the earthquake sequence including the Maple Creek A and B earthquakes. Also shown are double-couple source mechanisms for eleven  $M 2+$  (gray focal mechanisms) derived from HASH and the best fitting source mechanisms for the Maple Creek A and B earthquakes (black focal mechanisms) determined by our moment tensor inversion.

be near the brittle-ductile transition zone around the source region. In the transition zone of brittle-ductile deformation, a temperature is estimated to be  $\sim 400^\circ\text{C}$  in and around the Yellowstone caldera [Smith and Bruhn, 1984; Smith et al., 2009] where hydrothermal fluid should play an important role in the nucleation process of earthquakes.

[30] The source region of the Maple Creek A and B earthquakes also appears to be marked by a low  $P$  wave velocity ( $\sim 1.0\%$ ) [Husen et al., 2004a], although the depth of the low  $P$  wave velocity anomaly was not well constrained. Jung and Green [2004] proposed through laboratory experiments that a low seismic velocity anomaly area with high temperature can be explained by a spatial clustering of microcracks that makes fluid flow more likely. Although other explanations for the low  $P$  wave velocity anomaly are possible, our preferred interpretation is that the low  $P$  wave velocity anomaly around the source region represents a region of concentrated microcracks in a similar manner to Jung and Green [2004]. Jung and Green [2004] also found seismic events in samples whose nucleation process induces a shear faulting + tensile cracking, which is consistent with the best fitting source model for the Maple Creek B earthquake determined by our moment tensor inversion (Figure 9).

[31] We further infer that the absence of a coseismic volumetric change for the Maple Creek A earthquake is related to a temporal change in fracture permeability in the country rock surrounding the source region. In the later stage of the earthquake sequence, the fracture permeability could have been greater than in the first stage. We examined the predicted coseismic static stress change (Coulomb failure stress change)  $\Delta\sigma_{\text{CFF}}$  induced by the Maple Creek

A earthquake. Following King et al. [1994] and Harris [1998],  $\Delta\sigma_{\text{CFF}}$  can be expressed as

$$\Delta\sigma_{\text{CFF}} = \Delta\tau_s + \mu_f \left( \Delta\sigma_n - \frac{B}{3} \Delta\sigma_{kk} \right), \quad (4)$$

where  $\Delta\tau_s$  and  $\Delta\sigma_n$  are the shear and the fault normal stress changes, respectively.  $\mu_f$  is the frictional coefficient and  $B$  is the Skempton coefficient.  $\Delta\sigma_{kk}$  is the volumetric stress change. We assumed  $\mu_f = 0.75$  and  $B = 0.5$  [e.g., Roeloffs, 1996]. To calculate  $\Delta\tau_s$  and  $\Delta\sigma_n$ , we used an elastic half-space model [Okada, 1992] with the characteristic rupture dimension  $\tilde{L}$ , and the slip on the fault,  $D = M_0/\mu\tilde{L}^2$  [Aki and Richards, 1980]. Given  $\Delta\sigma = 1$  MPa, the estimated value of  $\tilde{L}$  for the Maple Creek A earthquake is 540 m using equation (3), and  $D$  is then estimated to be 5.4 cm, assuming  $\mu = 10$  GPa. We find that  $\Delta\sigma_{\text{CFF}}$  is as large as 0.05 MPa for sites several kilometers distant from the rupture area of the Maple Creek A earthquake. Elkhoury et al. [2006] showed that stress on the order of 0.01–0.1 MPa can cause changes in permeability of fractured rock. We hypothesize that the Maple Creek A earthquake created new microfractures near the source region, which in turn encouraged the tensile dislocation for the Maple Creek B earthquake.

[32] As noted above, a high-pressurized fluid injection should be needed to trigger an earthquake with coseismic volumetric change such as the Maple Creek B earthquake. The pressure gradient induced by the inflation of the magmatic sill, accompanying the 2004–2008 accelerated uplift episode, beneath the Yellowstone caldera could have caused subsurface fluid migrations outward to the Yellow-

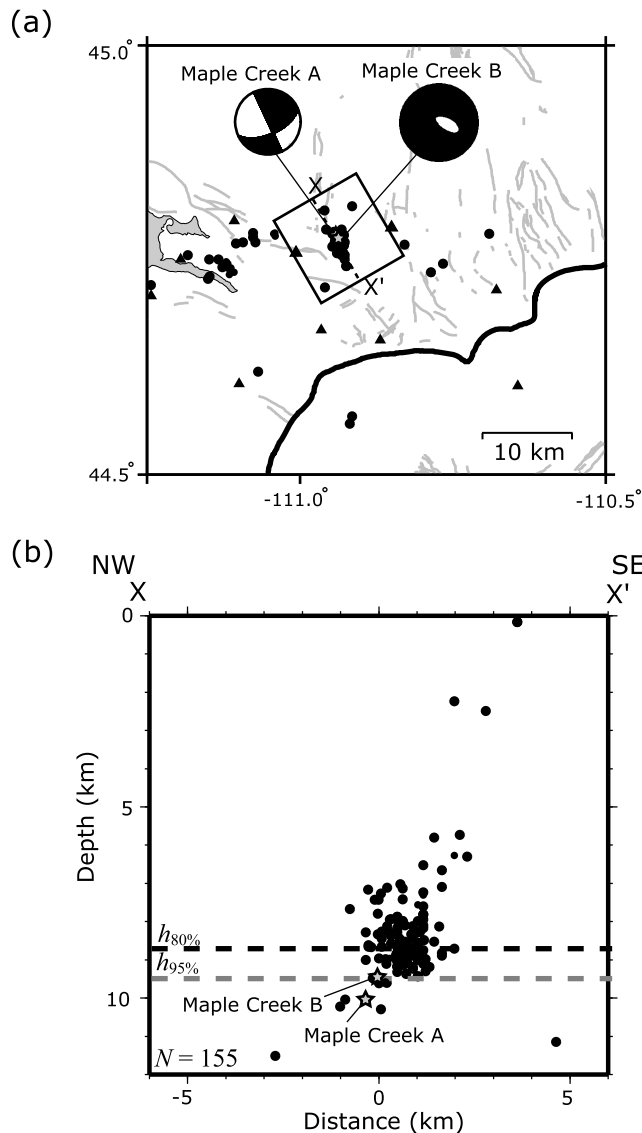


**Figure 11.** (a) Map view of the earthquake sequence including the Maple Creek A and B earthquakes during the time period of December 25, 2007 through January 15, 2008. Dots and triangles are the locations of earthquakes and seismometers (both short-period and broadband stations), respectively. Also shown are the 0.64 million year Yellowstone caldera boundary (solid black line) and the Quaternary faults (gray lines). (b) X–X' vertical cross section of the area shown by black rectangle in Figure 11a. Dashed black and gray lines are the depth of the brittle-ductile transition inferred from  $h_{80\%}$  and  $h_{95\%}$  (see text), respectively.

stone caldera. For example, the largest historic earthquake swarm in Yellowstone National Park (the autumn 1985 earthquake swarm), occurred at 5–10 km south of the source region of the Maple Creek A and B earthquakes, was interpreted as induced by a migration of hydrothermal fluid outward from the Yellowstone caldera, based on the observed rate of migration of seismicity and the association with a change in caldera deformation from uplift to subsi-

dence [Waite and Smith, 2002]. The estimated average rate of volumetric change accompanying the 2004–2008 caldera-wide crustal deformation was  $\sim 0.1 \text{ km}^3/\text{a}$  [Chang *et al.*, 2007], which is nearly an order of magnitude greater than those for earlier episodes of caldera deformation [e.g., Wicks *et al.*, 2006]. Given this high rate, it is reasonable to make a similar inference to the autumn 1985 earthquake swarm that pressure changes resultant from an inflating magma sill were sufficient to drive pressurized hydrothermal fluids from beneath the caldera into the source region.

[33] We show that the West Thumb and Maple Creek B earthquakes are the first dilatational source earthquakes to be identified in Yellowstone National Park since the monitoring of Yellowstone seismicity began in 1973. The lack of a high-quality broadband seismic network prior to the 2000s prevented assessments of moment tensors prior to this study. The subsurface dilatational deformations that we detected are important for hazard mitigation of Yellowstone National Park because dilatational source earthquakes may eventually be related and lead to hydrothermal explosions that are considered to be a serious hazard. If appropriate broadband seismic data are available, the moment tensor inversions with variable different source models that we used would help in the evaluation of dilatational dislocation components in earthquake source processes and may thus be useful for monitoring subsurface dilatational deformations and volcanic hazard assessment.

## 5. Conclusions

[34] We examined five  $M \geq 3$  earthquakes in Yellowstone National Park during the 2004–2008 period of accelerated uplift using moment tensor inversion. With the benefit of high-quality broadband seismic data, our inversion results revealed that the 5 November 2007  $M_w$  3.3 West Thumb and the 9 January 2008  $M_w$  3.8 Maple Creek B earthquakes experienced notable coseismic volumetric changes, suggesting injections of high-pressurized fluid in their earthquake source processes. The fluid migrations were likely induced by the inflation of the magmatic sill beneath the Yellowstone caldera that was modeled by GPS and InSAR measurements [Chang *et al.*, 2007].

[35] For the  $M_w$  3.3 West Thumb earthquake, a notable 60% isotropic expansion component was estimated with a 3.2 cm opening dislocation across the fault area of  $0.12 \text{ km}^2$ . The location of the  $M_w$  3.3 West Thumb earthquake is in an area of expected dilatational change ( $\sim 10$  microstrain) induced by the magmatic sill, which is consistent with the estimated isotropic expansion component in the source mechanism of the West Thumb earthquake. We suggest that the inflation of a magmatic sill which activated a pore pressure change (or a fluid migration) that encouraged the  $M_w$  3.3 West Thumb dilatational source earthquake.

[36] The estimated source mechanism for the  $M_w$  3.8 Maple Creek B earthquake is a combination of 70% normal faulting and 30% opening tensile component. The amount of the tensile (dilatational) dislocation is equivalent to a 3.3 cm opening crack over the fault area of  $0.58 \text{ km}^2$ . We propose that the coseismic stress change ( $\sim 0.05 \text{ MPa}$ ) resultant from the preceding  $M_w$  3.4 Maple Creek A earthquake created new microfractures that increased fracture permeability, coupled with pressurized fluids, induced a

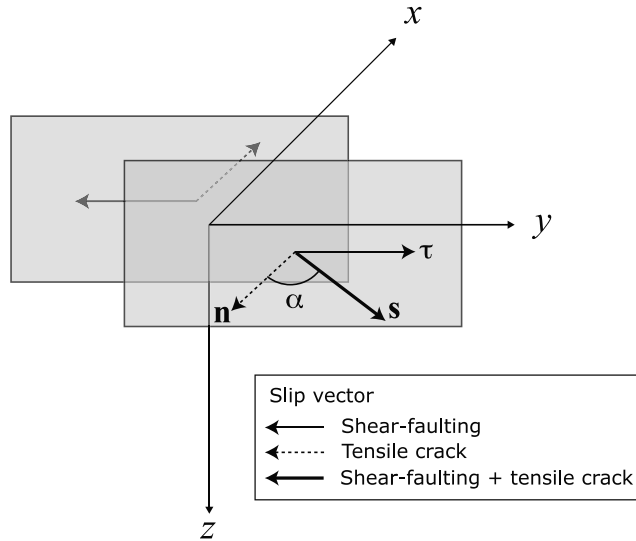


**Figure A1.** A schematic view of shear faulting + tensile crack source model;  $\tau$  is the slip vector of shear dislocation (arrow);  $\mathbf{n}$  is the normal vector to the shear plane (dashed arrow);  $\mathbf{s}$  is the slip vector of the described source model (solid arrow). The slip of tensile crack dislocation is parallel to the normal vector.

dilatational dislocation accompanying the  $M_w$  3.8 Maple Creek B earthquake.

## Appendix A: Shear-Faulting and Tensile Crack Source Model

[37] Following *Dufumier and Rivera* [1997] and *Minson et al.* [2007], we here describe moment tensor elements for a shear faulting + tensile crack source model. This source model is represented by a combination of one shear dislocation and one tensile dislocation. In the source model, the direction of tensile dislocation is normal to the shear plane (Figure A1). A slip vector of the source model  $\mathbf{s}$ , can be expressed by

$$\mathbf{s} = \cos \alpha \mathbf{n} + \sin \alpha \boldsymbol{\tau}, \quad (\text{A1})$$

where  $\mathbf{n}$  and  $\boldsymbol{\tau}$  are the normal vector to the shear plane and the slip vector of a shear dislocation, respectively;  $\alpha$  is the angle of  $\mathbf{s}$  from  $\mathbf{n}$  (Figure A1). For  $\alpha = 90^\circ$ , a source mechanism becomes a pure double couple while a pure tensile crack for  $\alpha = 0^\circ$  (opening crack) or  $\alpha = 180^\circ$  (closing crack). The seismic moment tensor  $\mathbf{M}$ , with a fault area  $S$ , and a slip  $D$ , is given by [*Aki and Richards*, 1980]

$$\mathbf{M} = SD[\lambda(\mathbf{s} \cdot \mathbf{n})\mathbf{I} + \mu(\mathbf{ns}^T + \mathbf{sn}^T)], \quad (\text{A2})$$

where the superscript T represents the vector transpose and the dot in the numerator denotes the *dot product*;  $\mathbf{I}$  is the identity matrix;  $\lambda$  and  $\mu$  are the Lamé constants, respectively. In a principal axes coordinate system,  $\mathbf{M}$  can be expressed by

$$\mathbf{M} = SD \begin{bmatrix} \lambda \cos \alpha + \mu(\cos \alpha - 1) & 0 & 0 \\ 0 & \lambda \cos \alpha & 0 \\ 0 & 0 & \lambda \cos \alpha + \mu(\cos \alpha + 1) \end{bmatrix}. \quad (\text{A3})$$

[38] The moment tensor decomposition of  $\mathbf{M}$  can be written as

$$\mathbf{M} = \mathbf{M}_{\text{DC}} + \mathbf{M}_{\text{TC}}, \quad (\text{A4})$$

where  $\mathbf{M}_{\text{DC}}$  and  $\mathbf{M}_{\text{TC}}$  are the moment tensors of shear and tensile dislocations, respectively. Using the fault orientation parameters: strike ( $\phi$ ) and dip ( $\delta$ ) of *Aki and Richards* [1980] with a Poisson solid (i.e.,  $\lambda = \mu$ ), moment tensor elements for  $\mathbf{M}_{\text{TC}}$  in Cartesian coordinates:

$$\mathbf{M}_{\text{TC}} = \begin{bmatrix} M_{xx}^{\text{TC}} & M_{xy}^{\text{TC}} & M_{xz}^{\text{TC}} \\ M_{xy}^{\text{TC}} & M_{yy}^{\text{TC}} & M_{yz}^{\text{TC}} \\ M_{xz}^{\text{TC}} & M_{yz}^{\text{TC}} & M_{zz}^{\text{TC}} \end{bmatrix}, \quad (\text{A5})$$

where

$$\begin{aligned} M_{xx}^{\text{TC}} &= (1 + 2 \sin^2 \delta \sin^2 \phi) M_{\text{TC}}, \\ M_{xy}^{\text{TC}} &= (-\sin^2 \delta \sin 2\phi) M_{\text{TC}}, \\ M_{yy}^{\text{TC}} &= (1 + 2 \sin^2 \delta \cos^2 \phi) M_{\text{TC}}, \\ M_{xz}^{\text{TC}} &= (\sin 2\delta \sin \phi) M_{\text{TC}}, \\ M_{yz}^{\text{TC}} &= (-\sin 2\delta \cos \phi) M_{\text{TC}}, \\ M_{zz}^{\text{TC}} &= (1 + 2 \cos^2 \delta) M_{\text{TC}}. \end{aligned} \quad (\text{A6})$$

Those for  $\mathbf{M}_{\text{DC}}$  can be seen in the work of *Aki and Richards* [1980] or *Lay and Wallace* [1995].

[39] From equation (A3), scalar seismic moments for double-couple  $M_{\text{DC}}$  ( $\alpha = 90^\circ$ ) and tensile crack  $M_{\text{TC}}$  ( $\alpha = 0^\circ$  or  $\alpha = 180^\circ$ ) components can be defined as

$$M_{\text{DC}} = \mu S D_{//}, \quad (\text{A7})$$

$$M_{\text{TC}} = \lambda S D_{\perp}, \quad (\text{A8})$$

where  $D_{//}$  and  $D_{\perp}$  are the fault parallel and the normal slip components of  $D$ , respectively.

[40] **Acknowledgments.** We thank the staff of the University of Utah seismograph stations for routinely picking arrival times of the Yellowstone earthquake catalog. The National Park Service cooperated in operating the Yellowstone seismic network. G. P. Waite provided a constructive review of an early draft of this manuscript. We would like to thank B. A. Chouet for providing us with the three-dimensional finite difference code and J. M. Farrell and J. C. Pechmann for discussions. Careful reviews by S. D. Malone and an anonymous reviewer greatly improved this manuscript. A software package, Generic Mapping Tools (GMT) [*Wessel and Smith*, 1998], was used for plotting figures. The present study was supported by the National Science Foundation Continental Dynamics Program under grant EAR-0314237 and The Brinson Foundation.

## References

- Aki, K., and P. G. Richards (1980), *Quantitative Seismology*, Freeman, New York.
- Benz, H. M., and R. B. Smith (1984), Simultaneous inversion for lateral velocity variations and hypocenters in the Yellowstone region using earthquake and refraction data, *J. Geophys. Res.*, *89*, 1208–1220, doi:10.1029/JB089iB02p01208.
- Bouchon, M., and K. Aki (1977), Discrete wave-number representation of seismic-source wave fields, *Bull. Seismol. Soc. Am.*, *67*, 259–277.
- Chang, W.-L., R. B. Smith, C. Wicks, J. M. Farrell, and C. M. Puskas (2007), Accelerated uplift and magmatic intrusion of the Yellowstone caldera, 2004 to 2006, *Science*, *318*, 952–956, doi:10.1126/science.1146842.

- Chouet, B. A. (1996), New methods and future trends in seismological volcano monitoring, in *Monitoring and Mitigation of Volcano Hazards*, edited by R. Scarpa and R. Tilling, pp. 23–97, Springer, New York.
- Christiansen, R. L. (2001), The Quaternary and Pliocene Yellowstone Plateau volcanic field of Wyoming, Idaho, and Montana, *U.S. Geol. Surv. Prof. Pap.*, 729-G, 1–145.
- Clawson, S. R., R. B. Smith, and H. M. Benz (1989), P wave attenuation of the Yellowstone caldera from three-dimensional inversion of spectral decay using explosion source seismic data, *J. Geophys. Res.*, 94(B6), 7205–7222, doi:10.1029/JB094iB06p07205.
- DeNosaquo, K. R., R. B. Smith, and A. R. Lowry (2009), Density and lithospheric strength models of the Yellowstone-Snake River Plain volcanic system from gravity and heat flow data, *J. Volcanol. Geotherm. Res.*, 188, 108–127, doi:10.1016/j.jvolgeores.2009.08.006.
- Doser, D. I. (1985), Source parameters and faulting processes of the 1959 Hebgen Lake, Montana, earthquake sequence, *J. Geophys. Res.*, 90(B6), 4537–4556, doi:10.1029/JB090iB06p04537.
- Dreger, D. S., H. Tkalčić, and M. Johnston (2000), Dilatational processes accompanying earthquakes in the Long Valley caldera, *Science*, 288, 122–125, doi:10.1126/science.288.5463.122.
- Dufumier, H., and L. Rivera (1997), On the resolution of the isotropic component in moment tensor inversion, *Geophys. J. Int.*, 131, 595–606, doi:10.1111/j.1365-246X.1997.tb06601.x.
- Dzurisin, D., K. M. Yamashita, and J. W. Kleinman (1994), Mechanisms of crustal uplift and subsidence at the Yellowstone caldera, Wyoming, *Bull. Volcanol.*, 56, 261–270, doi:10.1007/BF00302079.
- Efron, B. (1982), *The Jackknife, the Bootstrap and Other Resampling Plans*, Soc. for Ind. and Appl. Math., Philadelphia, Pa.
- Efron, B., and R. J. Tibshirani (1993), *An Introduction to the Bootstrap*, *Monogr. Stat. Appl. Probab.*, vol. 57, Chapman and Hall, New York.
- Elkhoury, J. E., E. E. Brodsky, and D. C. Agnew (2006), Seismic waves increase permeability, *Nature*, 441, 1135–1138, doi:10.1038/nature04798.
- Farrell, J., S. Husen, and R. B. Smith (2009), Earthquake swarm and b-value characterization of the Yellowstone volcano-tectonic system, *J. Volcanol. Geotherm. Res.*, 188, 260–276, doi:10.1016/j.jvolgeores.2009.08.008.
- Ford, S. R., D. S. Dreger, and W. R. Walter (2009), Identifying isotropic events using a regional moment tensor inversion, *J. Geophys. Res.*, 114, B01306, doi:10.1029/2008JB005743.
- Foulger, G. E., B. R. Julian, D. P. Hill, A. M. Pitt, P. E. Malin, and E. Shalev (2004), Non-double-couple microearthquakes at Long Valley caldera, California, provide evidence for hydraulic fracturing, *J. Volcanol. Geotherm. Res.*, 132, 45–71, doi:10.1016/S0377-0273(03)00420-7.
- Fournier, R. O. (1989), Geochemistry and dynamics of the Yellowstone National Park hydrothermal system, *Annu. Rev. Earth Planet. Sci.*, 17, 13–53, doi:10.1146/annurev.ea.17.050189.000305.
- Gottsmann, J., A. G. Camacho, K. F. Tiampo, and J. Fernández (2006), Spatiotemporal variations in vertical gravity gradients at the Campi Flegrei caldera (Italy): A case for source multiplicity during unrest?, *Geophys. J. Int.*, 167, 1089–1096, doi:10.1111/j.1365-246X.2006.03157.x.
- Hardebeck, J. L., and P. M. Shearer (2002), A new method for determining first-motion focal mechanisms, *Bull. Seismol. Soc. Am.*, 92, 2264–2276, doi:10.1785/0120010200.
- Harris, R. A. (1998), Introduction to special section: Stress triggers, stress shadows, and implications for seismic hazard, *J. Geophys. Res.*, 103(B10), 24,347–24,358, doi:10.1029/98JB01576.
- Hill, D. P., J. O. Langbein, and S. Prejean (2003), Relations between seismicity and deformation during unrest in Long Valley caldera, California, from 1995 through 1999, *J. Volcanol. Geotherm. Res.*, 127, 175–193, doi:10.1016/S0377-0273(03)00169-0.
- Husen, S., and R. B. Smith (2004), Probabilistic earthquake relocation in three-dimensional velocity models for the Yellowstone National Park region, Wyoming, *Bull. Seismol. Soc. Am.*, 94, 880–896, doi:10.1785/0120030170.
- Husen, S., R. B. Smith, and G. P. Waite (2004a), Evidence for gas and magmatic sources beneath the Yellowstone volcanic field from seismic tomographic imaging, *J. Volcanol. Geotherm. Res.*, 131, 397–410, doi:10.1016/S0377-0273(03)00416-5.
- Husen, S., S. Wiemer, and R. B. Smith (2004b), Remotely triggered seismicity in the Yellowstone National Park region by the 2002 Mw 7.9 Denali fault earthquake, Alaska, *Bull. Seismol. Soc. Am.*, 94, S317–S331, doi:10.1785/0120040617.
- Ichinose, G. A., J. G. Anderson, K. D. Smith, and Y. Zeng (2003), Source parameters of eastern California and western Nevada earthquakes from regional moment tensor inversion, *Bull. Seismol. Soc. Am.*, 93, 61–84, doi:10.1785/0120020603.
- Ide, S., G. C. Beroza, S. G. Prejean, and W. L. Ellsworth (2003), Apparent break in earthquake scaling due to path and site effects on deep borehole recordings, *J. Geophys. Res.*, 108(B5), 2271, doi:10.1029/2001JB001617.
- Jónsson, S. (2009), Stress interaction between magma accumulation and trapdoor faulting on Sierra Negra volcano, Galápagos, *Tectonophysics*, 471, 36–44, doi:10.1016/j.tecto.2008.08.005.
- Julian, B. R., and S. A. Sipkin (1985), Earthquake processes in the Long Valley caldera area, California, *J. Geophys. Res.*, 90(B13), 11,155–11,169, doi:10.1029/JB090iB13p11155.
- Julian, B. R., A. D. Miller, and G. R. Foulger (1998), Non-double-couple earthquakes: 1. Theory, *Rev. Geophys.*, 36, 525–549, doi:10.1029/98RG00716.
- Jung, H., and H. W. Green (2004), Experimental faulting of serpentinite during dehydration: Implications for earthquakes, seismic low-velocity zones, and anomalous hypocenter distributions in subduction zones, *Int. Geol. Rev.*, 46, 1089–1102, doi:10.2747/0020-6814.46.12.1089.
- Kanamori, H., G. Ekström, A. Dziewonski, J. S. Barker, and S. A. Sipkin (1993), Seismic radiation by magma injection: An anomalous seismic event near Tori Shima, Japan, *J. Geophys. Res.*, 98(B4), 6511–6522, doi:10.1029/92JB02867.
- King, G. C. P., R. S. Stein, and J. Lin (1994), Static stress changes and the triggering of earthquakes, *Bull. Seismol. Soc. Am.*, 84, 935–953.
- Lay, T., and T. C. Wallace (1995), *Modern Global Seismology*, Academic, London.
- Lomax, A., A. Zollo, P. Capuano, and J. Virieux (2001), Precise, absolute earthquake location under Somma-Vesuvius volcano using a new 3D velocity model, *Geophys. J. Int.*, 146, 313–331, doi:10.1046/j.0956-540x.2001.01444.x.
- Menke, W. (1989), *Geophysical Data Analysis: Discrete Inverse Theory*, Academic, San Diego, Calif.
- Miller, A. D., B. R. Julian, and G. R. Foulger (1998), Three-dimensional seismic structure and moment tensors of non-double-couple earthquakes at the Hengill-Grensdalur volcanic complex, Iceland, *Geophys. J. Int.*, 133, 309–325, doi:10.1046/j.1365-246X.1998.00492.x.
- Miller, D. S., and R. B. Smith (1999), P and S velocity structure of the Yellowstone volcanic field from local earthquake and controlled-source tomography, *J. Geophys. Res.*, 104(B7), 15,105–15,121, doi:10.1029/1998JB900095.
- Minson, S. E., D. S. Dreger, R. Bürgmann, H. Kanamori, and K. M. Larson (2007), Seismically and geodetically determined nondouble-couple source mechanisms from the 2000 Miyakejima volcanic earthquake swarm, *J. Geophys. Res.*, 112, B10308, doi:10.1029/2006JB004847.
- Morgan, P., D. D. Blackwell, R. E. Spafford, and R. B. Smith (1977), Heat flow measurements in Yellowstone Lake and the thermal structure of the Yellowstone caldera, *J. Geophys. Res.*, 82(26), 3719–3732, doi:10.1029/JB082i026p03719.
- Ohminato, T., and B. A. Chouet (1997), A free-surface boundary condition for including 3D topography in the finite difference method, *Bull. Seismol. Soc. Am.*, 87, 494–515.
- Okada, Y. (1992), Internal deformation due to shear and tensile faults in a half-space, *Bull. Seismol. Soc. Am.*, 82, 1018–1040.
- Pelton, J. R., and R. B. Smith (1979), Recent crustal uplift recent crustal uplift in Yellowstone National Park, *Science*, 206, 1179–1182, doi:10.1126/science.206.4423.1179.
- Pitt, A. M., C. S. Weaver, and W. Spence (1979), The Yellowstone Park earthquake of June 30, 1975, *Bull. Seismol. Soc. Am.*, 69, 187–205.
- Prejean, S. G., and W. L. Ellsworth (2001), Observations of earthquake source parameters at 2 km depth in the Long Valley caldera, eastern California, *Bull. Seismol. Soc. Am.*, 91, 165–177, doi:10.1785/0120000079.
- Puskas, C. M., R. B. Smith, C. M. Meertens, and W. L. Chang (2007), Crustal deformation of the Yellowstone–Snake River Plain volcano-tectonic system: Campaign and continuous GPS observations, 1987–2004, *J. Geophys. Res.*, 112, B03401, doi:10.1029/2006JB004325.
- Roeloffs, E. (1996), Poroelastic techniques in the study of earthquake-related hydrological phenomena, *Adv. Geophys.*, 37, 135–195.
- Roeloffs, E., M. Sneed, D. L. Galloway, M. L. Sorey, C. D. Farrar, J. F. Howle, and J. Hughes (2003), Water-level changes induced by local and distant earthquakes at Long Valley caldera, California, *J. Volcanol. Geotherm. Res.*, 127, 269–303, doi:10.1016/S0377-0273(03)00173-2.
- Rolandone, F., R. Bürgmann, and R. M. Nadeau (2004), The evolution of the seismic-aseismic transition during the earthquake cycle: Constraints from the time-dependent depth distribution of aftershocks, *Geophys. Res. Lett.*, 31, L23610, doi:10.1029/2004GL021379.
- Ross, A., G. R. Foulger, and B. R. Julian (1996), Non-double-couple earthquake mechanisms at the Geysers geothermal area, California, *Geophys. Res. Lett.*, 23, 877–880, doi:10.1029/96GL00590.
- Silver, P. G., and W. W. Chan (1991), Shear wave splitting and subcontinental mantle deformation, *J. Geophys. Res.*, 96(B10), 16,429–16,454, doi:10.1029/91JB00899.
- Smith, R. B., and W. J. Arabasz (1991), Seismicity of the intermountain seismic belt, in *Neotectonics of North America, Decade Map*, vol. 1,

- edited by D. B. Slemmons et al., pp. 185–228, Geol. Soc. of Am., Boulder, Colo.
- Smith, R. B., and R. L. Bruhn (1984), Intraplate extensional tectonics of the Eastern Basin-Range: Inferences on structural style from seismic reflection data, regional tectonics, and thermal-mechanical models of brittle-ductile deformation, *J. Geophys. Res.*, *89*(B7), 5733–5762, doi:10.1029/JB089iB07p05733.
- Smith, R. B., and M. Sbar (1974), Contemporary tectonics and seismicity of the western United States with emphasis on the Intermountain Seismic Belt, *Bull. Seismol. Soc. Am.*, *85*, 1205–1218.
- Smith, R. B., M. Jordan, B. Steinberger, C. M. Puskas, J. Farrell, G. P. Waite, S. Husen, W.-L. Chang, and R. O'Connell (2009), Geodynamics of the Yellowstone hotspot and mantle plume: Seismic and GPS imaging, kinematics, and mantle flow, *J. Volcanol. Geotherm. Res.*, *188*, 26–56, doi:10.1016/j.jvolgeores.2009.08.020.
- Templeton, D. C., and D. S. Dreger (2006), Non-double-couple earthquakes in the Long Valley volcanic region, *Bull. Seismol. Soc. Am.*, *96*, 69–79, doi:10.1785/0120040206.
- Vasco, D. W., C. M. Puskas, R. B. Smith, and C. M. Meertens (2007), Crustal deformation and source models of the Yellowstone volcanic field from geodetic data, *J. Geophys. Res.*, *112*, B07402, doi:10.1029/2006JB004641.
- Waite, G. P., and R. B. Smith (2002), Seismic evidence for fluid migration accompanying subsidence of the Yellowstone caldera, *J. Geophys. Res.*, *107*(B9), 2177, doi:10.1029/2001JB000586.
- Waite, G. P., and R. B. Smith (2004), Seismotectonics and stress field of the Yellowstone volcanic plateau from earthquake first-motion and other indicators, *J. Geophys. Res.*, *109*, B02301, doi:10.1029/2003JB002675.
- Waite, G. P., R. B. Smith, and R. M. Allen (2006),  $V_p$  and  $V_s$  structure of the Yellowstone hot spot from teleseismic tomography: Evidence for an upper mantle plume, *J. Geophys. Res.*, *111*, B04303, doi:10.1029/2005JB003867.
- Wessel, P., and W. H. F. Smith (1998), New, improved version of generic mapping tools released, *Eos Trans. AGU*, *79*(47), 579, doi:10.1029/98EO00426.
- Wicks, C., W. Thatcher, and D. Dzurisin (1998), Migration of fluids beneath Yellowstone caldera inferred from satellite radar interferometry, *Science*, *282*, 458–462, doi:10.1126/science.282.5388.458.
- Wicks, C., W. Thatcher, D. Dzurisin, and J. Svarc (2006), Uplift, thermal unrest, and magma intrusion at Yellowstone caldera, *Nature*, *440*, 72–75, doi:10.1038/nature04507.
- Yuan, H., and K. Dueker (2005), Teleseismic P wave tomogram of the Yellowstone plume, *Geophys. Res. Lett.*, *32*, L07304, doi:10.1029/2004GL022056.
- Zoback, M. L., and M. D. Zoback (1989), Tectonic stress field of the conterminous United States, in *Geophysical Framework of the Continental United States*, edited by L. C. Pakiser and W. D. Mooney, *Mem. Geol. Soc. Am.*, *172*, 523–539.

---

W.-L. Chang, Department of Earth Sciences, National Central University, 300 Jhongda Rd., Jhongli City, Taoyuan 32001, Taiwan. (wuchang@ncu.edu.tw)

R. B. Smith, Department of Geology and Geophysics, University of Utah, 135 South 1460 East, Salt Lake City, UT 84112, USA. (rbsmith@mines.utah.edu)

T. Taira, Berkeley Seismological Laboratory, University of California, 215 McCone Hall, Berkeley, CA 94720, USA. (taira@seismo.berkeley.edu)